Hindawi
Journal of Applied Mathematics
Volume 2023, Article ID 7882843, 10 pages
https://doi.org/10.1155/2023/7882843

Research Article

Predicting COVID-19 Pandemic Endpoint in Some Sub-Saharan African and European Countries

Saviour Worlanyo Akuamoah,[1] **John Coker Ayimah**,[1] **David Yaro**,[2] **Elikem Kofi Krampa**,[1] **and Awura Amma Adomaa Danso**[1]

[1]*Faculty of Applied Sciences and Technology, Ho Technical University, P. O. Box HP 217, Ho, Ghana*
[2]*School of Applied Sciences and Technology, Cape Coast Technical University, P. O. Box DL 50, Ghana*

Correspondence should be addressed to Saviour Worlanyo Akuamoah; wakuamoah@htu.edu.gh

Received 9 September 2022; Revised 9 December 2022; Accepted 10 January 2023; Published 24 January 2023

Academic Editor: Fernando Simoes

In this study, a novel modified SIR model is presented with two control measures to predict the endpoint of COVID-19, in top three sub-Saharan African countries (South Africa, Ethiopia, and Kenya) including Ghana and top four European countries (France, Germany, UK, and Italy). The reproduction number's sensitivity indices with regard to the model parameters were explicitly derived and then numerically evaluated. Numerical simulations of the suggested optimal control schemes in general showed a continuous result of decline at different anticipated extinction timelines. Another interesting observation was that in the simulation of sub-Saharan African dynamics, it was observed that the use of personal protective equipment was more effective than the use of vaccination, whereas in Europe, the use of vaccination was more effective than personal protective equipment. From the simulations, the conclusion is that COVID-19 will end before the 3rd year in Ghana, before the 6th year in Kenya, and before the 9th year in both Ethiopia and South Africa.

1. Introduction

The severe acute respiratory syndrome coronavirus-2 (SARS-CoV-2) epidemic that led to the new coronavirus disease-2019 (COVID-19) outbreak first started in Wuhan in the Chinese province of Hubei [1]. Due to its high rates of infection and transmission, COVID-19 has gained international attention [2]. The World Health Organization proclaimed it as a worldwide pandemic on March 11, 2020 (World Health Organization 2020).

Dealing with the novel coronavirus is one of the new worldwide problems in infectious disease management in 2019. The most typical symptoms within two to fourteen days are fever, exhaustion, dry cough, myalgia, and dyspnea [3]. The infectious COVID-19 illness severely disrupted daily life all around the world because of its quick pandemic potential and lack of vaccines and medications. Currently, the coronavirus has killed more than 6,488,644 individuals, infected more than 606,100,742 people, and forced more than 6 billion people to remain in their homes for sometime [4].

Several researchers have adopted an individual-level strategy that looks for the overall average equilibrium [5–7], where individuals may choose their contact rate and are motivated by various initiatives to compare the overall average equilibrium to a socially optimum approach. Additionally, data-based strategies like those in [8–11] have offered intriguing insights into the effectiveness of stay-at-home directives and target lock downs. Further theoretical research on COVID-19 [12–17] has indeed been helpful in understanding the dynamics of transmission and the potential role of various effective interventions, like mitigation and suppression to slow down the epidemic's spread, the demand for health precautions to maintain those who are prone to various risks from infections, the number of infective cases to the low level, enforcing lockdown on regions of highly infective cases, home isolation of suspected cases, and home quarantine.

The phenomenon exhibits can be modeled as ordinary differential equations (ODEs) and may be solved using a variety of analytical and numerical techniques. This makes Susceptible ⟶ Infectious ⟶ Recovery (SIR) models computationally effective and permits the study of huge regions of parameter space relatively fast. In order to develop and analyze preventative and control strategies for decreasing the spread of infectious diseases and containing unwanted social behavior, mathematical modeling has become an essential tool [18–20], and most of these models are based on the SIR model. The reproduction number, R_0 measures the rate at which the disease spread is adopted in controlling a virus. Anderson and May [12] estimated that each virus has a unique value for R_0 (for example, the R_0 value for influenza spread is 3).

The ultimate goal of control methods for many infectious diseases is eradication, which is complete removal of the pathogen from the host populations and the environment. However, strong preventative efforts have been stepped up in recent years to stop further transmission [21–25].

Nonetheless, the main motivation for this work is to propose a modified SIR model to predict the endpoint of COVID-19 in three most endemic sub-Saharan African countries (South Africa, Ethiopia, and Kenya) including Ghana and four most infested European countries (France, Germany, UK, and Italy).

At recent study, Kumar et al. [24] used autoregressive integrated moving average (ARIMA) and machine learning to forecast the dynamics of COVID-19 pandemic in top most 15 countries. For the first time, we have proposed a novel modified SIR model to predict the endpoint of COVID-19.

We design a novel Susceptible ⟶ Infectious ⟶ Quarantined ⟶ Susceptible (SIQS) model for COVID-19 to examine its stability characteristics in relation to its threshold parameters. We then investigate the model's stability properties without the use of control measures and perform further analyses on the model to find the reproduction number R_0. The optimal control measures were also imposed on the model. To analyze the numerical simulations, we establish the model parameters. Finally, the results were discussed and conclusions made.

The results of this study, we think, will be useful for policy evaluation to end the current and future spread of COVID-19.

2. The Proposed Method

The SIR model simulates the time-histories of an epidemic phenomenon. It simulates the mutual and dynamic interaction of humans in three different conditions: susceptible (S), infective (I), and recovered (R). For this model, we assume that births and deaths occur at equal rate and that all newborns are susceptible (no inherited immunity). We denote the rate at which individuals are born into the susceptible class with no passive as $\mu^* N$ and average death rate by μ. We also assume the population mix homogeneously, with no restriction of age, mobility, or other social factors.

From Figure 1, we let the rate at which the susceptible enters the infectious stage to be βSI and the rate at which an infected individual may recover at quarantine αI and become susceptible again at γQ_R. Also, the newly introduced population that arrived in the country and are yet to join the general public move directly into the quarantined compartment at a rate of $N(1-\mu^*)$.

Following the recent publications by Peng et al. [21], who researched into the COVID-19 infection in different Chinese provinces, we utilized a generalized SIR model to deduce the compartmental ODE model as shown below:

$$\begin{aligned} \frac{dS}{dt} &= \mu N - \beta SI - \mu S + \gamma Q, \\ \frac{dI}{dt} &= \beta SI - (\mu + \alpha) I, \\ \frac{dQ}{dt} &= N(1-\mu) + \alpha I - (\gamma + \mu) Q. \end{aligned} \tag{1}$$

The transmission coefficient is $\beta > 0$, the latency coefficient $\alpha > 0$, the recovery coefficient $\gamma > 0$, and the capital death rate $\mu > 0$. From Equation (1) the ODEs show that $S^1 + I^1 + R^1 = 0$; hence, the total population $N = S + I + R$.

This shows that the total population is constant; normalizing the system, we have

$$\begin{aligned} s(t) &= \frac{S(t)}{N}, \\ i(t) &= \frac{I(t)}{N}, \\ q(t) &= \frac{Q(t)}{N}. \end{aligned} \tag{2}$$

From Equation (1), the ODE can then be represented as

$$\begin{aligned} s' &= \mu - \beta si - \mu s + \gamma q, \\ i' &= \beta si - (\mu + \alpha) i, \\ q' &= (1-\mu) + \alpha i - (\gamma + \mu) q. \end{aligned} \tag{3}$$

3. Model Analysis

3.1. Disease-Free Equilibrium ($i = 0$). We get the explicit solution of the disease-free equilibrium point by solving Equation (3) as

$$(s^*, i^*, q^*) = \left(\frac{\mu^2 + \gamma}{\mu(\gamma + \mu)}, 0, \frac{1-\mu}{\gamma + \mu} \right). \tag{4}$$

3.2. Basic Reproductive Number

Theorem 1. *The disease-free equilibrium is locally stable if $R_0 < 1$ and unstable if $R_0 > 1$.*

Proof. By using the next-generation matrix approach (NGM) $= \mathrm{FV}^{-1}$, we reorder the above equation to get the Jacobian

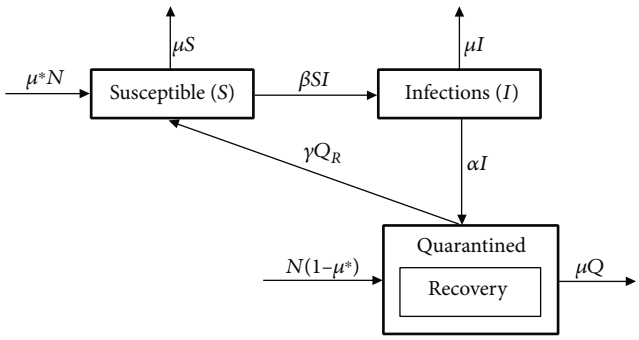

Figure 1: A conceptual diagram of the mathematical model for COVID-19.

matrix as

$$\text{JDFE} = \begin{pmatrix} -\beta i - \mu & -\beta s & \gamma \\ \beta i & \beta s - (\mu + \alpha) & 0 \\ 0 & \alpha & -(\gamma + \mu) \end{pmatrix}. \tag{5}$$

But at the disease-free equilibrium $(s^*, i^*, q^*) = ((\mu^2 + \gamma)/(\mu(\gamma + \mu)), 0, (1 - \mu)/(\gamma + \mu))$, this implies

$$\text{JDFE} = \begin{pmatrix} -\mu & -\dfrac{\beta(\mu^2 + \gamma)}{\mu(\gamma + \mu)} & \gamma \\ 0 & \dfrac{\beta(\mu^2 + \gamma)}{\mu(\gamma + \mu)} - (\mu + \alpha) & 0 \\ 0 & \alpha & -(\gamma + \mu) \end{pmatrix}. \tag{6}$$

Thus,

$$\begin{aligned} \text{JDFE} &= \begin{pmatrix} -\dfrac{\beta(\mu^2 + \gamma)}{\mu(\gamma + \mu)} & 0 \\ 0 & 0 \end{pmatrix} - \begin{pmatrix} 0 & -\gamma \\ -\alpha & (\gamma + \mu) \end{pmatrix}, \\ \text{FV}^{-1} &= \begin{pmatrix} \dfrac{\beta(\mu^2 + \gamma)}{\mu\gamma\alpha} & \dfrac{\beta(\mu^2 + \gamma)}{\mu\alpha(\gamma + \mu)} \\ 0 & 0 \end{pmatrix}. \end{aligned} \tag{7}$$

Consequently, R_0 is the most dominant eigenvalues of the NGM; hence,

$$R_0 = \frac{\beta(\mu^2 + \gamma)}{\mu\gamma\alpha}. \tag{8}$$

The disease-free equilibrium eigenvalues are

$$\begin{aligned} \lambda_1 &= -\mu, \\ \lambda_2 &= -\mu - \alpha, \\ \lambda_3 &= -\frac{\alpha\gamma\mu + \alpha\mu^2 - \beta\mu^2 + \gamma\mu^2 + \mu^3 - \beta\gamma}{\mu(\gamma + \mu)}, \end{aligned} \tag{9}$$

and since eigenvalues of the characteristic equations are all negative, the system's disease-free equilibrium is locally asymptotically stable. As a result, if $R_0 < 1$, then the equilibrium point is locally stable, and if $R_0 > 1$, then it is unstable. This completes the proof. □

3.3. An Endemic Equilibrium Point ($i \neq 0$). At the endemic equilibrium, we assume that there are infections present in the population; hence, we have

$$\begin{aligned} s^* &= \frac{\mu + \alpha}{\beta}, \\ i^* &= \frac{-\mu^3 + \mu - \alpha(R_0 - 1)}{\mu\beta(\gamma + \alpha + \mu)}, \\ q^* &= \frac{(-\beta - \alpha)\mu^2 + (-\alpha^2 + \beta)\mu + \alpha\beta}{\mu\beta(\gamma + \alpha + \mu)}. \end{aligned} \tag{10}$$

Theorem 2. *The endemic equilibrium is locally stable if $R_0 < 1$ and unstable if $R_0 > 1$.*

Proof. To prove this, we consider Equation (3) about the endemic equilibrium points; after doing the necessary substitutions into the Jacobian matrix (5), we have

$$J_{EE} = \begin{pmatrix} \dfrac{\mu^3 - \mu + \alpha(R_0 - 1)}{\mu(\gamma + \alpha + \mu)} - \mu & -(\mu + \alpha) & \gamma \\ \dfrac{\mu^3 - \mu + \alpha(R_0 - 1)}{\mu(\gamma + \alpha + \mu)} & 0 & 0 \\ 0 & \alpha & -(\gamma + \mu) \end{pmatrix}. \tag{11}$$

Dividing the matrix into three 2×2 matrices, namely, d_1, d_2, and d_3, we solve for the eigenvalues of the Jacobian matrix at the endemic equilibrium:

$$\begin{aligned} \det(J - \lambda I) = &\left(\left(\frac{\mu^3 - \mu + \alpha(R_0 - 1)}{\mu(\gamma + \alpha + \mu)} - \mu\right) - \lambda\right) \\ &\times d_1 + (\mu + \alpha) \times d_2 + \gamma \times d_3. \end{aligned} \tag{12}$$

The characteristic polynomial was obtained in the form

$$\lambda^3 + \lambda^2 b_1 + \lambda b_2 + b_3 = 0, \tag{13}$$

with

$$\begin{aligned} b_1 &= (\gamma + \mu), \\ b_2 &= \mu^2 + \gamma\mu - \left(\frac{\mu^3 - \mu + \alpha(R_0 - 1)}{\mu(\gamma + \alpha + \mu)}\right)(\alpha - \gamma), \\ b_3 &= \mu^3 - \mu + \alpha(R_0 - 1). \end{aligned} \tag{14}$$

Using the Routh-Hurwitz stability criteria, if the coefficients of the characteristic equation $b_1 > 0$, $b3 > 0$, and $b_1 b_2 - b3 > 0$ are true, then all the roots of the

characteristic equation have negative real parts which means a stable equilibrium [26]. □

3.4. Sensitivity Analysis. We further explore the sensitivity of the reproductive generation number R_0 to better understand the model dynamics and assess the robustness of the model predictions with regard to parameter values. These indices show how responsive R_0 is to each parameter change. A positive sensitivity index shows an increase or (decrease) in the parameter value whereas a negative sensitivity index suggests a decrease (increase) in the value of R_0. Figure 2 shows a contour plot dynamics of R_0 in terms of the controllable parameters α and μ. We derive the sensitivity of R_0 with respect to β,μ, γ, and α as shown in Figure 3.

Remark 3. The sensitivity index of a normalized forward variable say Q that depends differentially on a parameter w is defined as

$$\frac{\partial Q}{\partial w} \times \frac{w}{Q}. \tag{15}$$

It can be observed that viral infection of healthy individuals μ_2, recovered individual rate from quarantined γ_2, and per capita rate of COVID-19 virus production (β) have sensitivity index of +1. This means that increasing (decreasing) these parameters by 10% will lead to a corresponding 10% increase (decreases) in R_0. Conversely, the death rate of individuals μ_1, those in susceptible after recovering γ_1, and death rate α of those quarantined have sensitivity index of -1. This means that increasing (decreasing) these parameters by 10% will lead to a corresponding 10% decreases (increases) in R_0. The above remarks suggest control strategies that will effectively reduce the infection rate of individual per capita rate of COVID-19 virus production.

3.5. Optimal Control Measures. Here, we extend our model in Equation (1) by including two time-dependent control measures, namely,

(i) $v_1(t)$: personal protective equipment, commonly referred to as "PPE," is an equipment worn to minimize exposure to COVID-19

(ii) $v_2(t)$: vaccinations for COVID-19 have effectiveness rates ranging from 60 to 94 percent [4]. COVID-19 vaccinations should have at least 50% effectiveness against severe illness, according to World Health Organization recommendations

It is anticipated that the accompanying force of persuasion to COVID-19 in the general population is lowered by a factor of $(1 - v_1(t))$ as more people gain access to education on the effective use of the PPE. Furthermore, the number of infected COVID-19 is lowered by a factor of $(e + \alpha v_2(t))$ as more infected individuals transition to the recovery compartment, where e is the rate of spontaneous

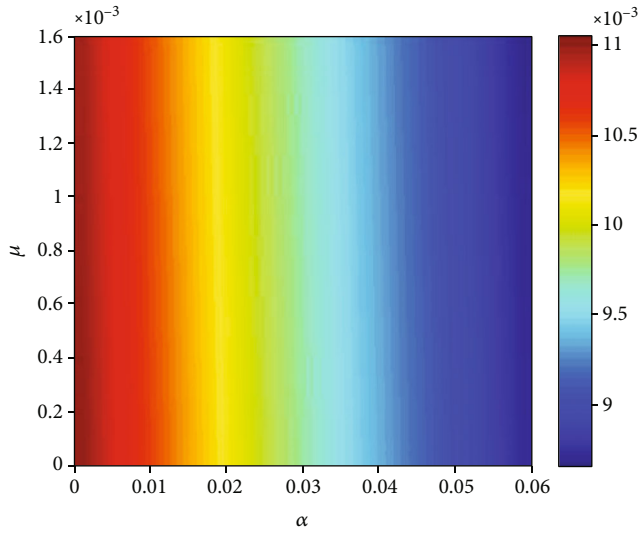

Figure 2: Contour plot of R_0 in terms of the controllable parameters: α (rate of recovery) and μ (the birth rate of individuals).

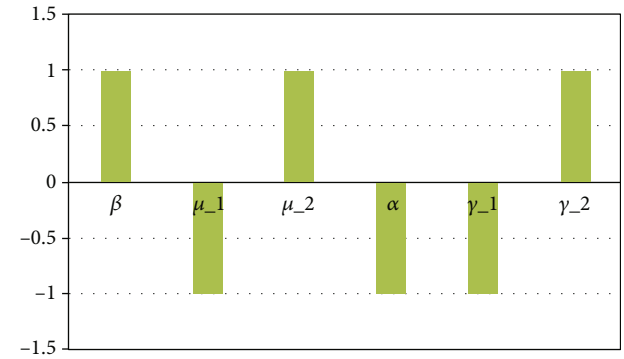

Figure 3: Sensitivity indices for R_0 with respect to the model parameters.

recovery. Equation (1) can therefore be rewritten as

$$\begin{aligned}
\frac{dS}{dt} &= \mu N - (1 - v_1(t))\beta SI - \mu S + \gamma Q,\\
\frac{dI}{dt} &= (1 - v_1(t))\beta SI - (e + \alpha v_2(t))I - \mu I,\\
\frac{dQ}{dt} &= N(1 - \mu) + (e + \alpha v_2(t))I - (\gamma + \mu)Q.
\end{aligned} \tag{16}$$

We then define the objective function as

$$J(v_1, v_2) = \int_0^{\tau} \left(k_1 I + k_2 v_1^2 + k_3 v_2^2\right) dt. \tag{17}$$

The coefficients k_1, k_2, and k_3 are positive weights with the final time as τ. The main objective is to minimize the infectious rate among the general population in addition to also minimizing the cost in using PPE.

We denote the cost incurred by infected individuals as $k_1 I$, while $k_2 v_1^2$ is the cost associated with PPE and $k_3 v_2^2$ is the cost of vaccinations for COVID-19 to the general public. We established optimal controls v_1^* and v_2^* such that

$$J(v_1^*, v_2^*) = \min_{(v_1, v_2)} \{J(v_1, v_2) | v_1, v_2 \in \Omega\}, \tag{18}$$

with the control set

$$\Omega = \{(v_1, v_2) | v_i : [0, \tau] \longrightarrow [0, \infty) \quad \text{Lebesgue measurable}, i = 1, 2\}. \tag{19}$$

Using Pontryagin's maximum principle necessary conditions satisfying optimal control [27], we convert Equations (16) and (17) into a point-wise equation. Minimizing the Hamiltonian H with respect to (v_1, v_2) gives

$$\begin{aligned} H = {} & k_1 I + k_2 v_1^2 + k_3 v_2^2 + \Delta_S[\mu N - (1 - v_1(t))\beta SI - \mu S + \gamma Q] \\ & + \Delta_I[(1 - v_1(t))\beta SI - (e + \alpha v_2(t))I - \mu I] \\ & + \Delta_Q[N(1 - \mu) + (e + \alpha v_2(t))I - (\gamma + \mu)Q], \end{aligned} \tag{20}$$

where Δ_S, Δ_I, and Δ_Q are the costate variables [21]

$$\begin{aligned} \frac{\partial H}{\partial S} &= -\frac{d\Delta_S}{dt} = (\mu N - 1 + v_1(t))\beta I\Delta_s - \mu + (1 - v_1(t))\beta I\Delta_I, \\ \frac{\partial H}{\partial I} &= -\frac{d\Delta_I}{dt} = k_1 - (1 + v_1(t))\beta S\Delta_S \\ &\quad - (v_1(t)\beta S + e + \alpha v_2(t) + \mu)\Delta_I + \Delta_Q(e + \alpha v_2(t)), \\ \frac{\partial H}{\partial Q} &= -\frac{d\Delta_Q}{dt} = \Delta_S\gamma - (1 + \mu)\Delta_Q. \end{aligned} \tag{21}$$

In our model, we set a boundary condition for the final time as τ since there are no final values for the state variables to have

$$\Delta_S(\tau) = \Delta_I(\tau) = \Delta_Q(\tau) = 0. \tag{22}$$

The control set for the interior $0 < v_i < 1$, where $i = 1, 2$, is given by

$$\begin{aligned} \frac{\partial H}{\partial v_1} &= 2k_2 v_1 + \beta SI(\Delta_s - \Delta_I) = 0, \\ \frac{\partial H}{\partial v_2} &= 2k_3 v_2 - \alpha I(\Delta_Q - \Delta_I) = 0, \end{aligned} \tag{23}$$

resulting in

$$\begin{aligned} v_1 &= \frac{\beta SI(-\Delta_s + \Delta_I)}{2k_2}, \\ v_2 &= \frac{\alpha I(\Delta_Q + \Delta_I)}{2k_3}. \end{aligned} \tag{24}$$

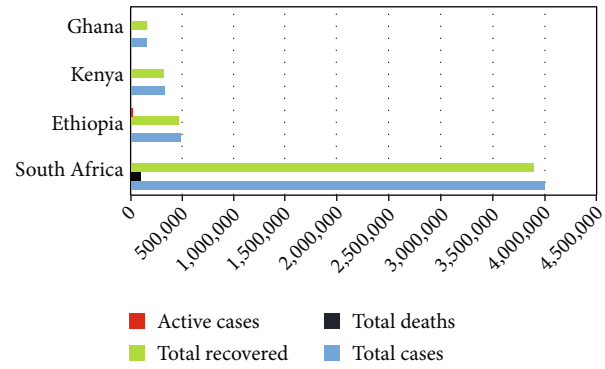

Figure 4: Total reported cases due to COVID-19, 14 July 2022.

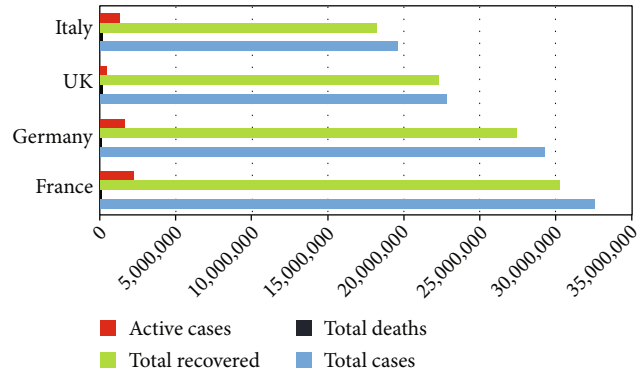

Figure 5: Total reported cases due to COVID-19, 14 July 2022.

By using common control arguments that include the limits of the control variables, we conclude that

$$\begin{aligned} v_1^* &= \min\left[1, \max\left(0, \frac{\beta SI(-\Delta_s + \Delta_I)}{2k_2}\right)\right], \\ v_2^* &= \min\left[1, \max\left(0, \frac{\alpha I(\Delta_Q + \Delta_I)}{2k_3}\right)\right]. \end{aligned} \tag{25}$$

4. Determination of Model Parameters

Using similar techniques in Amdouni et al. [28] and Chitnis et al. [29], the COVID-19 model parameters were obtained out of the three highest recording countries in sub-Saharan African countries (South Africa, Ethiopia, and Kenya) including Ghana and European countries (France, Germany, UK, and Italy) from Worldometer as shown in Figures 4 and 5.

4.1. Estimating Values for N. From the sub-Saharan African data, which comprises of South Africa, Ethiopia, Kenya, and Ghana, an average of 999836, 122704, 84111, and 41804, respectively, are born into the susceptible compartment every year at a rate of 2737, 336, 230, and 114, respectively. We assume that these numbers are not fixed; hence, we explored the following ranges 2500-3000, 300-350, 200-250, and 100-150, respectively.

Likewise for the following European countries (France, Germany, UK, and Italy), we have respective averages 22279, 20060, 15663, and 13461 individuals being born into

Table 1: Summary of the estimated parameters. Data obtained from https://www.worldometers:info=coronavirus=#maintable.

Parameters	South Africa	Ethiopia	Kenya	Ghana	France	Germany	UK	Italy
β = Total cases/Population	0.066	0.004	0.006	0.005	0.50	0.35	0.33	0.33
α = Total active cases/Total recovered	0.97	0.95	0.98	0.99	0.93	0.94	0.97	0.93
γ = Total recovered/Total cases	0.007	0.004	0.006	0.005	0.91	0.50	0.49	0.45
μ = Total death/Total cases	0.002	0.00006	0.0001	0.00004	0.002	0.001	0.003	0.003

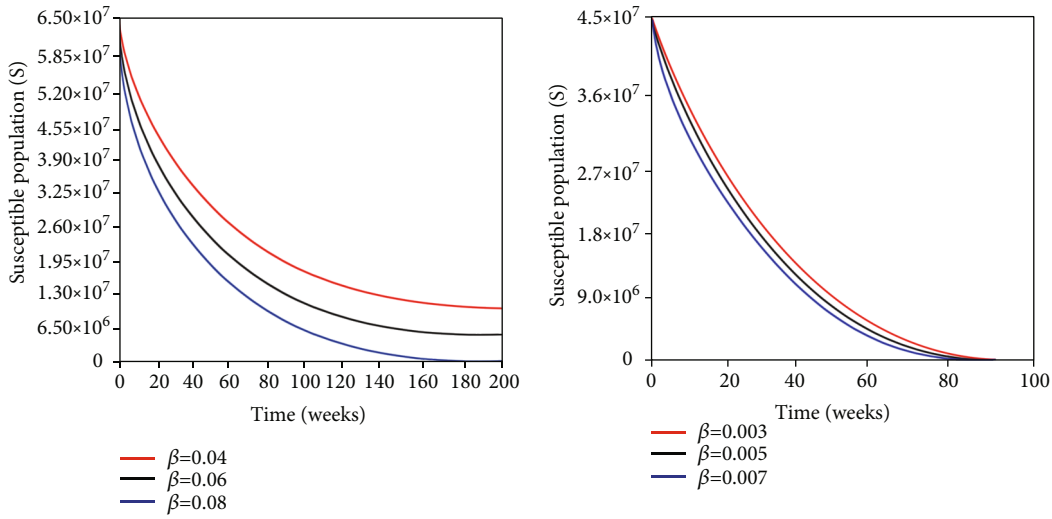

(a) Results of varying β values on S

(b) Results of varying β values on S

Figure 6: Varying β values for sub-Saharan African countries.

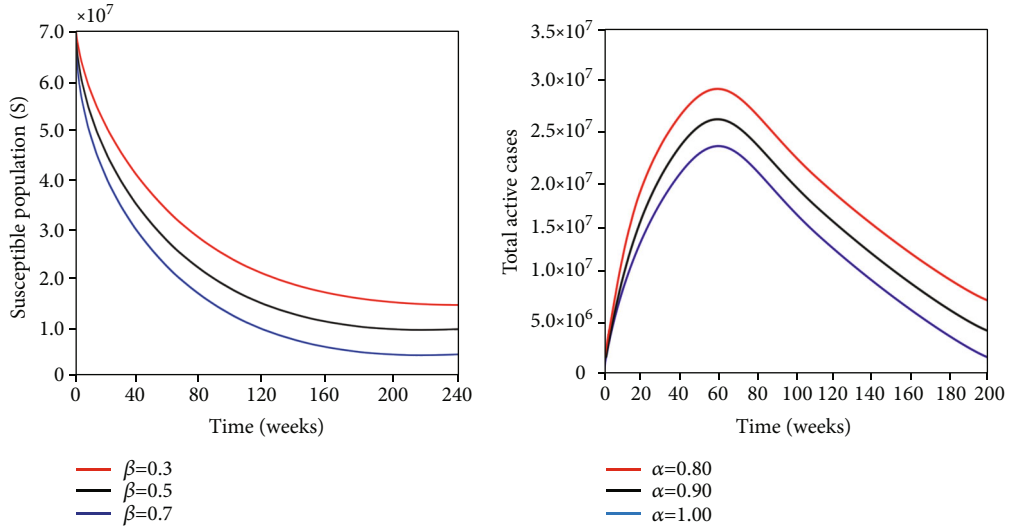

(a) Results of varying β values on S

(b) Results of varying α values on R

Figure 7: Varying β and α values for European countries.

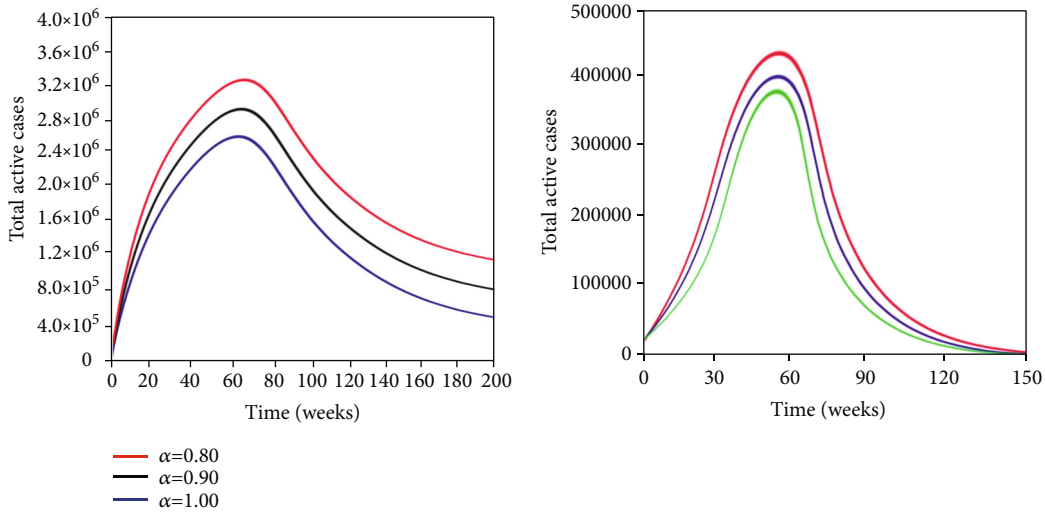

(a) Results of varying α values on R (b) Results of varying α values on R

FIGURE 8: Varying α values for total active cases in sub-Saharan Africa.

the susceptible compartment. Again, we assume the following ranges: 20000-25000, 1800-23000, 13000-18000, and 10000-15000.

5. Numerical Simulations

Numerical simulations were employed in this section to demonstrate how parameter modifications and the impact of the two ideal control measures affect the dynamics of the system as well as the values of the reproduction numbers.

From Table 1, the reproduction number takes the value $Ro = 3.568$, and in using the realistic initial values and parameter settings from Table 1, the behavior of the model system, Equation (1), is numerically examined using boundary value problem MATLAB ODE4 (MATLAB BVP4C) together with boundary conditions $t = 0$ and $t = \tau$.

The effects of changing β values (the contact rate between susceptible and infectious population) are shown in Figures 6 and 7(a) for the various selected sub-Saharan African and European countries, while keeping the remaining parameters in Table 1 constant. It was found out that the susceptible population decreases as β rates increases, which is a result of a more susceptible population coming into contact with infectious population. In Figure 7(b) for the selected European countries and Figure 8 for the various selected sub-Saharan African countries, the infectious population decreases as the recovery rate α increases.

To demonstrate the effect of the optimal control strategies on the prevalence of COVID-19 among the susceptible population, the optimal control applies both control measures simultaneously to control the prevalence of COVID-19 in the population. Without the controls, that is, if $v_1 = 0$ and $v_2 = 0$, Figure 9 demonstrates a considerable increase in the susceptible population. In cases where $v_1 = 0$ and $v_2 \neq 0$ or $v_1 \neq 0$ and $v_2 = 0$, the susceptible population grows more quickly and achieves a greater peak before gradually declining to a lower level.

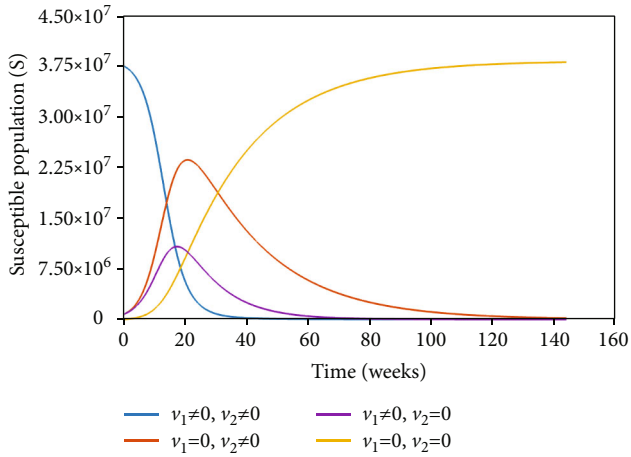

FIGURE 9: Control measures for sub-Saharan Africa.

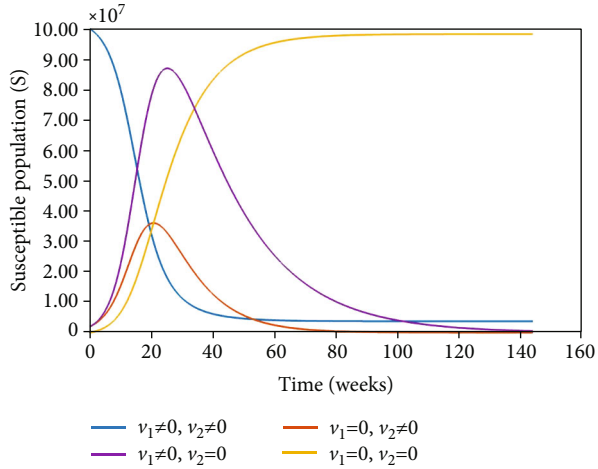

FIGURE 10: Control measures for Europe.

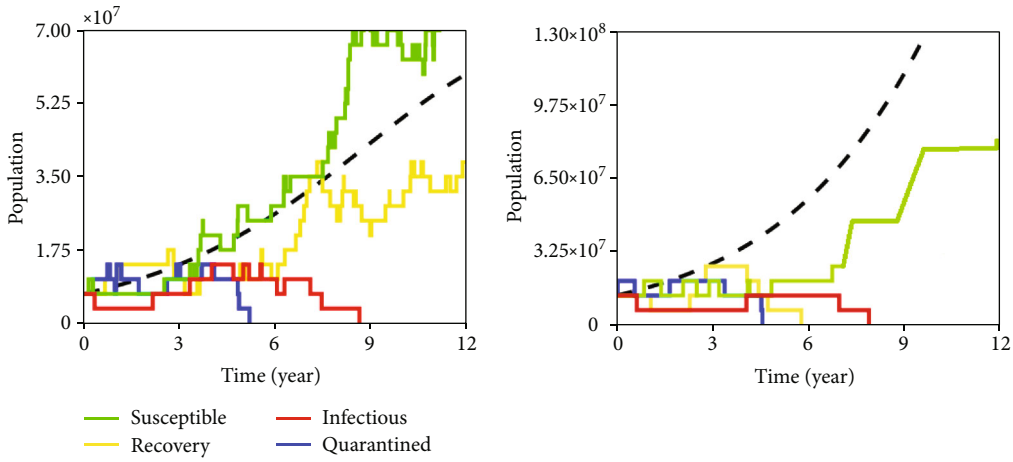

(a) South Africa (b) Ethiopia

Figure 11: Trend of COVID-19 cases for the next twelve years.

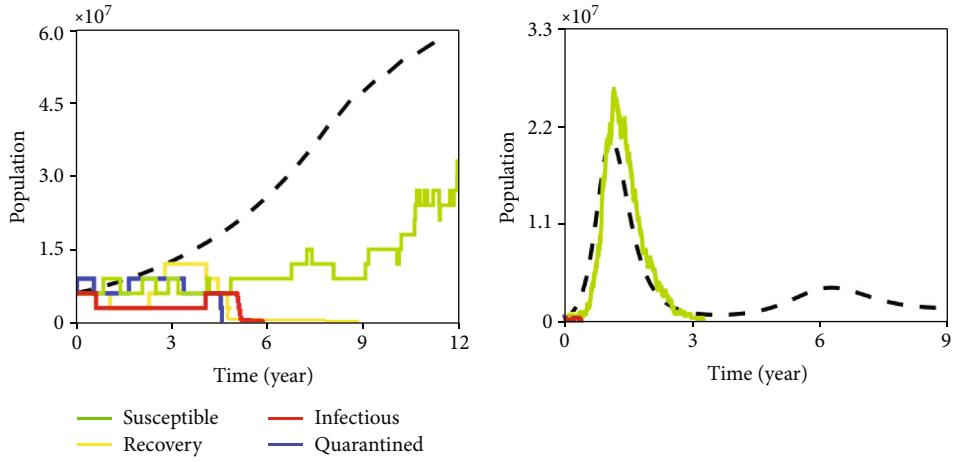

(a) Kenya (b) Ghana

Figure 12: Trend of COVID-19 cases for the next twelve years.

The control profile $v_1 \neq 0$ and $v_2 \neq 0$ in Figure 9 begins at the upper bound and progressively descends to the lower level, in Figure 10, if $v_1 = 0$ and $v_2 = 0$, showing a considerable increase. Again in cases where $v_1 = 0$ and $v_2 \neq 0$ or $v_1 \neq 0$ and $v_2 = 0$, the susceptible population increases more quickly and achieves a greater peak before declined to a lower level.

The control profile for Europe begins at the upper boundary and slowly decreases to a steady lower level at relatively longer periods. The two figures indicate that the use of PPE and vaccinations for COVID-19 drastically reduces the spread of the disease.

Using the SIQS model, we have predicted some trajectory for the four sub-Saharan African and the four European countries in the upcoming years. The strategies for controlling contagious diseases were employed as a control measure, and in general, the simulations in Figures 11–14 showed a continuous result of decline at different anticipated extinction timelines. Another interesting observation was that in the sub-Saharan Africa countries' simulation, it was observed that the use of PPE was more effective than the use of vaccination, whereas in Europe, the use of vaccination was more effective than PPE.

The simulation for South Africa and Ethiopia in Figure 11 showed a total eradication of COVID-19 before the ninth year. The recovery rate for South Africa increases in the coming years as compared to Ethiopia, Kenya, and Ghana. In Figure 12, the rate of spread for Kenya disappears suddenly before the 6th year and before the 3rd year in Ghana. From Figure 13, the disease will be extinct in France and Germany prior to the 8th year; in the UK, spread will continue after the 8th year and become extinct just before the 9th year. However, in Italy, the disease will eventually die out after the 4th year.

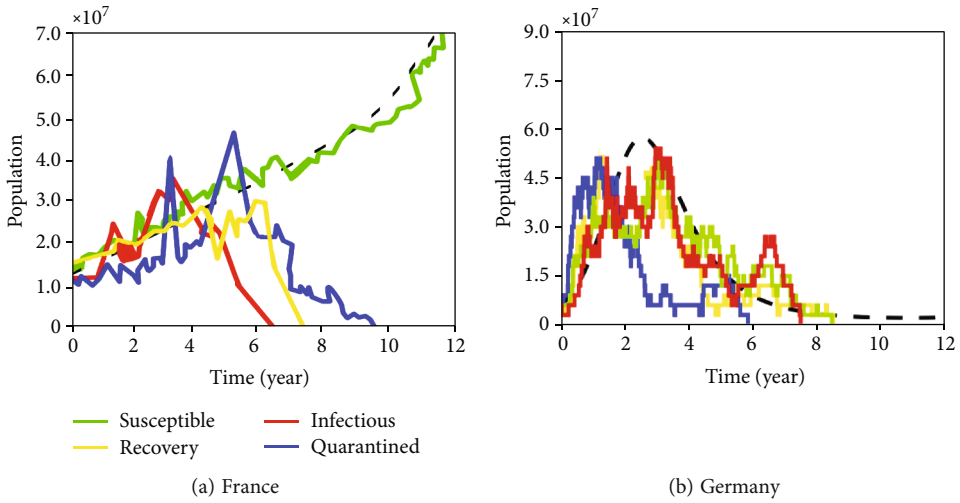

(a) France (b) Germany

Figure 13: Trend of COVID-19 cases for the next twelve years.

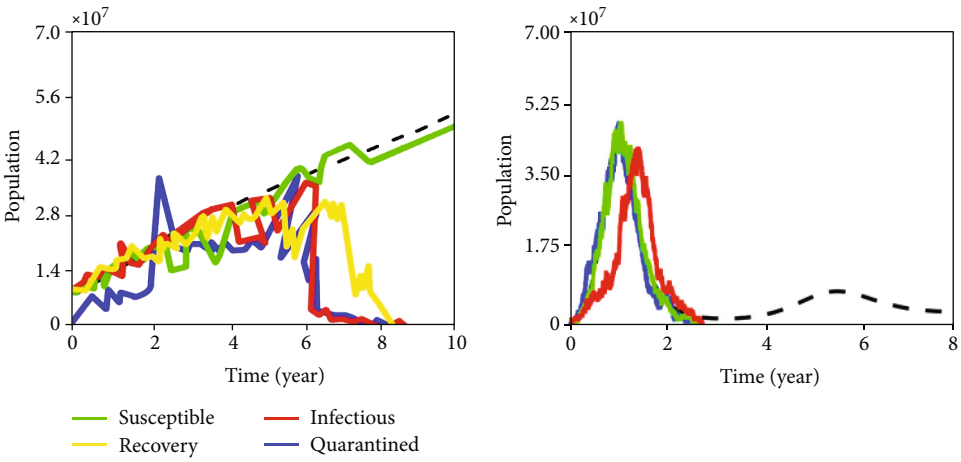

(a) UK (b) Italy

Figure 14: Trend of COVID-19 cases for the next twelve years.

6. Conclusion and Recommendations

The main aim of this work was to propose a modified SIR model to predict the extinction of COVID-19 in four most dominant sub-Saharan African countries (South Africa, Ethiopia, Kenya, and Ghana) and European countries (France, Germany, UK, and Italy). The susceptible population's growth and decline were represented by the basic reproduction number R_0 in epidemic models. The susceptible equilibrium is found to be stable if $R_0 < 1$ and unstable if $R_0 > 1$.

The reproduction number's sensitivity indices with regard to the model parameters were explicitly derived and then numerically evaluated. Two time-dependent controls were included in the model to evaluate how to manage the spread of the disease. Additionally, we used graphical plots to explore the function of the contact rate γ along with other important characteristics like the recovery rate α. After the analyses and simulations, it was observed that, in the long run, the disease will become extinct much more earlier in Ghana and in Italy. Another interesting observation was that in the sub-Saharan Africa countries, it was realized that the use of PPE was more effective than the use of vaccines, whereas in Europe, the use of vaccines was more effective than PPE.

This study has a number of limitations, for instance, we avoided social distancing and the use of machine learning. Bayesian analysis as in Taimoor et al. [8] with SIR model would be considered in our modified paper to determine the endpoints of contagious diseases.

Data Availability

The data collected for this study can be obtained from the first author upon a reasonable request.

Conflicts of Interest

The authors declare that they have no conflict of interest regarding the publication of the research article.

References

[1] M. Lipsitch, D. L. Swerdlow, and L. Finelli, "Defining the epidemiology of Covid-19 — studies needed," *New England Journal of Medicine*, vol. 382, no. 13, pp. 1194–1196, 2020.

[2] N. Usman, M. A. Mamun, and I. Ullah, "COVID-19 infection risk in Pakistani health-care workers: the cost-efective safety measures for developing countries," *Social Health and Behavior*, vol. 3, no. 3, pp. 75–77, 2020.

[3] C. Huang, Y. Wang, X. Li et al., "Clinical features of patients infected with 2019 novel coronavirus in Wuhan, China," *The Lancet*, vol. 395, no. 10223, pp. 497–506, 2020.

[4] World Health Organization (WHO), *Novel Coronavirus (COVID-19) Situation*, WHO, Geneva, Switzerland, 2022, https://experience.arcgis.com/experience/685d0ace521648f8a5beeeee1b9125cd.

[5] A. Aurell, R. Carmona, G. Dayanikli, and M. Lauriere, "Optimal incentives to mitigate epidemics: a Stackelberg mean field game approach," 2021, https://arxiv.org/abs/2011.03105.

[6] S. Cho, "Mean-field game analysis of SIR model with social distancing," 2020, https://arxiv.org/abs/2005.06758.

[7] R. Elie, E. Hubert, and G. Turinici, "Contact rate epidemic control of COVID-19: an equilibrium view," *Mathematical Modelling of Natural Phenomena*, vol. 15, p. 35, 2020.

[8] M. Taimoor, S. Ali, I. Shah, and F. Roland Muwanika, "COVID-19 pandemic data modeling in Pakistan using time-series SIR," *Computational and Mathematical Methods in Medicine*, vol. 2022, Article ID 6001876, 14 pages, 2022.

[9] J. H. Fowler, S. J. Hill, R. Levin, and N. Obradovich, "Stay-at-home orders associate with subsequent decreases in COVID-19 cases and fatalities in the United States," *PLoS One*, vol. 16, no. 6, article e0248849, 2021.

[10] A. Fokas, J. Cuevas-Maraver, and P. Kevrekidis, "Easing COVID-19 lockdown measures while protecting the older restricts the deaths to the level of the full lockdown," *Scientific Reports*, vol. 11, no. 1, 2021.

[11] T. C. Reluga, "Game theory of social distancing in response to an epidemic," *PLoS Computational Biology*, vol. 6, no. 5, article e1000793, 2010.

[12] R. M. Anderson and R. M. May, *Infectious Diseases of Humans Dynamics and Control*, Oxford University Press, Oxford, UK, 1991.

[13] D. Yaro, W. O. Apeanti, S. W. Akuamoah, and D. Lu, "Analysis and optimal control of fractional-order transmission of a respiratory epidemic model," *International Journal of Applied and Computational Mathematics*, vol. 5, no. 4, p. 116, 2019.

[14] M. Maleewong, "Time delay epidemic model for COVID-19," *MedRxiv BMJ Yale*, vol. 15, pp. 1–8, 2020.

[15] J. Menéndez, "Elementary time-delay dynamics of COVID-19 disease," *MedRxiv BMJ Yale*, vol. 3, pp. 1–8, 2020.

[16] B. Ivorra, M. R. Ferrández, M. Vela-Pérez, and A. M. Ramos, "Mathematical modeling of the spread of the coronavirus disease 2019 (COVID-19) taking into account the undetected infections. The case of China," *Communications in Nonlinear Science and Numerical Simulation*, vol. 88, p. 105303, 2020.

[17] J. Arino and S. Porteta, "A simple model for COVID-19," *Infectious Disease Modelling*, vol. 5, pp. 309–315, 2020.

[18] H. Zhang, P. Harvim, and P. Georgescu, "Preventing the spread of schistosomiasis in Ghana: possible outcomes of integrated optimal control strategies," *Journal of Biological Systems*, vol. 25, no. 4, pp. 625–655, 2017.

[19] O. Okosun, O. Rachid, and M. Nizar, "Optimal control strategies and cost-effectiveness analysis of a malaria model," *Biosystems*, vol. 111, no. 2, pp. 83–101, 2013.

[20] C. Castillo-Chavez and B. Song, "Dynamical models of tuberculosis and their applications," *Mathematical Biosciences and Engineering*, vol. 1, no. 2, pp. 361–404, 2004.

[21] L. Peng, W. Yang, D. Zhang, C. Zhuge, and L. Hong, "Epidemic analysis of COVID-19 in China by dynamical modeling," 2020, https://arxiv.org/abs/2002.06563.

[22] A. R. Hinman, "Global progress in infectious disease control," *Vaccine*, vol. 16, no. 11-12, pp. 1116–1121, 1998.

[23] D. R. Hopkins, "Disease eradication," *The New England Journal of Medicine*, vol. 368, no. 1, pp. 54–63, 2013.

[24] P. Kumar, H. Kalita, S. Patairiya et al., "Forecasting the dynamics of COVID-19 pandemic in top 15 countries in April 2020: ARIMA model with machine learning," *Approach BMJ Yale*, vol. 4, pp. 1–14, 2020.

[25] G. T. Nieddu, L. Billings, J. H. Kaufman, E. Forgoston, and S. Bianco, "Extinction pathways and outbreak vulnerability in a stochastic Ebola model," *Journal of The Royal Society Interface*, vol. 14, 2017.

[26] A. Waris, A. U. Khan, M. Ali, A. Ali, and A. Baset, "COVID-19 outbreak: current scenario of Pakistan," *New Microbes and New Infections*, vol. 35, article 100681, 2020.

[27] L. S. Pontryagin, V. G. Boltyanskii, R. V. Gamkrelidze, and E. F. Mishchenko, *The Mathematical Theory of Optimal Processes*, Wiley, New York, NY, USA, 1962.

[28] B. Amdouni, M. Paredes, C. Kribs-Zaleta, and A. Mubayi, "Why do students quit school? Implications from a dynamical modelling study," *Proceedings of the Royal Society A: Mathematical, Physical and Engineering Sciences*, vol. 473, no. 2197, article 20160204, 2017.

[29] N. Chitnis, J. M. Hyman, and J. M. Cushing, "Determining important parameters in the spread of malaria through the sensitivity analysis of a mathematical model," *Bulletin of Mathematical Biology*, vol. 70, no. 5, pp. 1272–1296, 2008.